Proximity-induced giant spin-orbit interaction in epitaxial graphene on a topological insulator

Kyung-Hwan Jin[1] and Seung-Hoon Jhi[1,2]

[1]*Department of Physics, Pohang University of Science and Technology, Pohang 790-784, Republic of Korea*

[2]*Division of Advanced Materials Science, Pohang University of Science and Technology, Pohang 790-784, Republic of Korea*

(Received 2 June 2012; revised manuscript received 30 November 2012; published 26 February 2013)

Heterostructures of Dirac materials such as graphene and topological insulators provide interesting platforms to explore exotic quantum states of electrons in solids. Here we study the electronic structure of the graphene-Sb_2Te_3 heterostructure using density functional theory and tight-binding methods. We show that the epitaxial graphene on Sb_2Te_3 turns into the quantum spin-Hall phase due to its proximity to the topological-insulating Sb_2Te_3. It is found that the epitaxial graphene develops a giant spin-orbit gap of about ∼20 meV, which is about three orders of magnitude larger than that of pristine graphene. We discuss the origin of such enhancement of the spin-orbit interaction and possible outcomes of the spin-Hall phase in graphene.

DOI: 10.1103/PhysRevB.87.075442 PACS number(s): 73.22.Pr, 73.40.Mr, 75.70.Tj

I. INTRODUCTION

Heterojunctions of materials with different physical properties have served as a basis for finding new physical states and understanding complex phenomena in condensed matter systems. Diffusion of the order parameters by proximity induces a weak order in the nonordered materials, generating quantum interference effects. For example, supercurrents and interference effects due to the Josephson tunneling were observed in graphene in contact with superconductors, restoring the weak localization in graphene.[1,2] Recently topological insulators, which refer to the states of matter with insulating gaps in the bulk and gapless helical states on the surface, have attracted great attention due to their intriguing electronic structures. Dictated by time-reversal symmetry, the helical surface states termed massless Dirac fermions can move without backscattering on the surface of topological insulators. Heterojunctions of materials with different topological orders can thus provide an interesting platform to explore emerging quantum phenomena of Dirac fermions at the interfaces. For example, it was proposed that exotic particles such as the axion, magnetic monopole, and Majorana fermion can be realized in hybrid structures of topological insulator–superconductor or topological insulator–ferromagnets.[3,4]

Graphene is a representative Dirac material and has low-energy states with pseudohelicity and linear energy-momentum dispersion originating from the atomic symmetry. It is appropriate to ask what proximity effects can occur in graphene in contact with topological insulators (TIs). Does the strong spin-orbit interaction in TIs affect the electronic structure of graphene? Kane and Mele studied the possibility of a spin-Hall phase in graphene by introducing an orbital-symmetry and time-reversal-symmetry preserving term.[5] However, the strength of spin-orbit coupling (SOC) in graphene is extremely small and the spin-Hall phase is expected to occur at very low temperatures of a few kelvins.[6–9] The intrinsic and Rashba spin-orbit interactions in pristine graphene arise from hybridization between the π and σ bands.[6] Enhancing the hybridization, for instance, by adsorbing hydrogen adatoms, has been suggested to increase the SOC in graphene,[10] or simply adsorbing heavy elements such as thallium on graphene was proposed to induce the spin-Hall phase in graphene.[11]

From other perspectives, direct measurements of transport characteristics of TI surface states, which are crucial for developing the TI devices,[12] have been tried after verification of TI surface states by angle-resolved photoemission spectroscopy.[13–15] However, in most TI materials, the Fermi level lies in the conduction bands or valence bands[15,16] and the bulk conduction dominates over the conduction via the surface states. Ca- or Mn-doping or by intercalation have been tested to align the chemical potential in the middle of the TI bulk energy gap.[14,15] Being a truly 2D material with conducting channels that have linear energy dispersion, graphene is expected to be an ideal match to the TI surface states. In contact with TI surfaces, graphene is likely to be affected mostly by the TI surface states and thus to work as a probe to measure any changes in electrical conduction through the surface states. In this paper, we studied the electronic structure of epitaxial graphene on topological insulating Sb_2Te_3 using pseudopotential density functional theory and the tight-binding methods including the spin-orbit interactions. In particular we investigated the proximity effect in the graphene-TI junction and possible spin-Hall phases arising in graphene. By doing so, we also explore graphene-TI hybrid structures as devices to detect the helical surface states.

II. COMPUTATIONAL METHOD

First-principles calculations based on density functional theory were carried out using the Vienna *Ab initio* Simulation Package.[17] The exchange-correlation interaction of electrons was treated within the generalized gradient approximation (GGA) of the Perdew-Burke-Ernzerhof type.[18] Pseudopotentials generated by the projector augmented wave method were used for atomic potentials. The SOC was included at the second variational step using the scalar-relativistic eigenfunctions as a basis. A cutoff energy of 400 eV was used for the expansion of wave functions and potentials in the plane-wave basis. The k-point meshes of $11 \times 11 \times 1$ were used for the sampling of the Brillouin zone. For emulating the graphene-Sb_2Te_3 surface, we used the supercell method by putting a single layer of graphene on top of a Sb_2Te_3 slab and introducing a vacuum layer of 20 Å thickness between the cells to minimize artificial intercell interactions. Once full atomic relaxation was done, one additional step of self-consistent calculation was carried

out including the SOC until the total energy converges to within 10^{-5} eV. Electronic band structures from first-principles calculations were then fitted by tight-binding methods including SOC to analyze the origin of energy splitting.

III. RESULTS AND DISCUSSION

The epitaxial graphene on top of the Sb_2Te_3 surface was modeled by putting a single layer of graphene on a Sb_2Te_3 slab of 1 $\sim$ 5 quintuple layers (QLs) with Te atoms at the top [Fig. 1(a)]. We chose the experimental in-plane lattice constant of 4.25 Å for Sb_2Te_3[19] and then adjusted the lattice constant of graphene accordingly. The lattice mismatch by this choice is about $\sim$1% when we used a $\sqrt{3} \times \sqrt{3}$ in-plane supercell for graphene. We considered three atomic stacking configurations between graphene and Sb_2Te_3 as shown in Fig. 1: surface Te atoms at the center of carbon hexagon rings (P1), carbon atoms on top of surface Te atoms (P2), and carbon-carbon bridges on top of surface Te atoms (P3). In order to describe the van der Waals–type interaction between graphene and the TI surface, we employed a semiempirical correction by Grimme's method[20] because GGA cannot describe the van der Waals interaction correctly. We found that the P1 configuration is the most stable among the three.

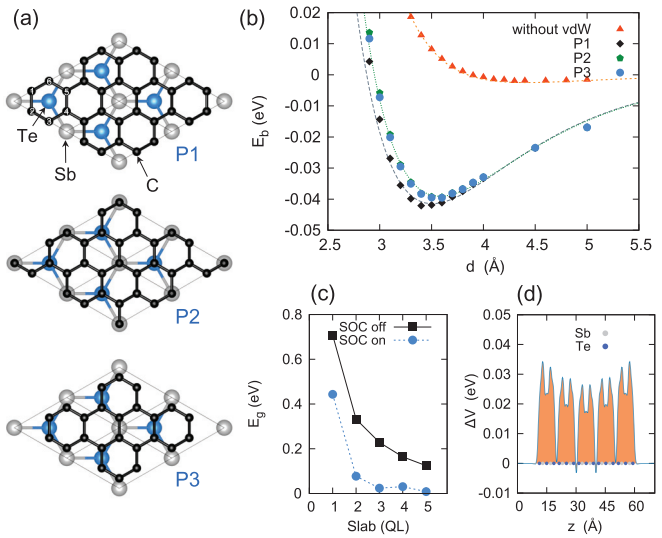

FIG. 1. (Color online) (a) Top views of atomic structures of epitaxial graphene on (111) surface of Sb_2Te_3 thin film (slab) modeled by $\sqrt{3} \times \sqrt{3}$ $R30^\circ$ supercell. Three contact configurations from top to bottom: P1, carbon hexagon centers on top of surface Te atoms (blue balls); P2, carbon atoms (gray balls) on top of surface Te atoms; P3, carbon-carbon bridges on top of surface Te atoms. (b) Calculated binding energy curves of graphene on Sb_2Te_3 with vdW interactions included as a function of binding distance (d). Without van der Waals corrections, GGA cannot describe the binding correctly. (c) Calculated (indirect) band gaps of Sb_2Te_3 slabs using first-principles methods including SOC (blue circles) and without it (filled boxes) as a function of slab thickness. (d) The differences in electrostatic potentials ($\Delta V = V_{so} - V_{sp}$) with and without SOC from our first-principles calculations of 5QL Sb_2Te_3 slab, where V_{so} and V_{sp} are the Hartree potentials including SOC and including only spin polarization without SOC, respectively.

Helical surface states of the topological-insulating phase start to appear over certain thicknesses of TI slabs. The TI surface states are fully developed in the Sb_2Te_3 slab of 3QL or thicker, which is common to other topological-insulating binary chalcogen compounds such as Bi_2Se_3 and Bi_2Te_3.[21,22] Figure 1(b) shows the calculated binding energy curves [$E_b = E_{\text{gra-TI}} - (E_g + E_{\text{TI}})$; E_{gra}-TI, E_g, and E_{TI} represent the cohesive energies of graphene-TI (3QL), graphene, and TI (3QL), respectively] with SOC and van der Waals interaction included. The equilibrium binding distance and energy in the P1 configuration are 3.48 Å and about $\sim$41 meV per carbon, respectively. We note that SOC does not affect the binding energy and distance. TI slabs still show a very small but finite energy gap due to the interaction between the surface states at two surfaces of the slabs.[21–23] Figure 1(c) shows our calculated band gaps of Sb_2Te_3 as the number of QLs is increased. Without SOC included, the band gap is large for thin slabs due to the quantum confinement effect and then converges to the bulk band gap as the thickness is increased. When SOC is included, the band gap decreases rapidly with increasing slab thickness. Figure 1(d)) shows the electrostatic potential difference (ΔV) in 5QL Sb_2Te_3, which represents a change in potential at the surfaces due to the SOC. The electric field by the potential gradient near the surfaces induces the Rashba splitting in graphene.

Now we studied the changes in the graphene electronic structure induced by TI contact. By increasing the slab thickness from 1QL to 4QL, we investigated how emerging TI surface states start to interact with graphene π bands. Our calculated band structures are shown in Fig. 2. A single layer of graphene with a $\sqrt{3} \times \sqrt{3}$ unit cell should have fourfold-degenerate Dirac cones at the Γ point due to band folding. On TI substrates (>3QL) with SOC, we observed a few intriguing features in the graphene Dirac cones: small-gap opening at the Dirac point, splitting in the fourfold-degenerate bands particularly in the valence bands, a change in the dispersion of the conduction bands, and the Rashba-type splitting in both the conduction and valence bands. The splitting of the valence bands is of particular interest as its size increases from 25, 41, 47, 52 meV for 1QL, 2QL, 3QL, and 4QL Sb_2Te_3, respectively (it is about 53 meV for 5QL). Without SOC, we do not observe such features in the Dirac cone of graphene except the small-gap opening at the Dirac point (Fig. 3). This observation of band splitting along with the Rashba-type splitting indicates that SOC and the inversion symmetry-breaking by TI substrate are playing the major role for the change of the graphene Dirac cones.

In order to understand and resolve the changes in the graphene band structure, we used the tight-binding Hamiltonian of Kane and Mele,[24,25] which includes both intrinsic and extrinsic SOC terms. The Hamiltonian for a 2D honeycomb lattice is given as

$$H = -t \sum_{\langle ij \rangle} c_i^\dagger c_j + \frac{i V_{SO}}{\sqrt{3}} \sum_{\langle\langle ij \rangle\rangle} c_i^\dagger \vec{\sigma} \cdot (\vec{d}_{kj} \times \vec{d}_{ik}) c_j + i V_R \sum_{\langle ij \rangle} c_i^\dagger \hat{e}_z \cdot (\vec{\sigma} \times \vec{d}_{ij}) c_j + i V_{Rh} \sum_{\langle ij \rangle} c_i^\dagger \hat{e}_\rho \cdot (\vec{\sigma} \times \vec{d}_{ij}) c_j .$$

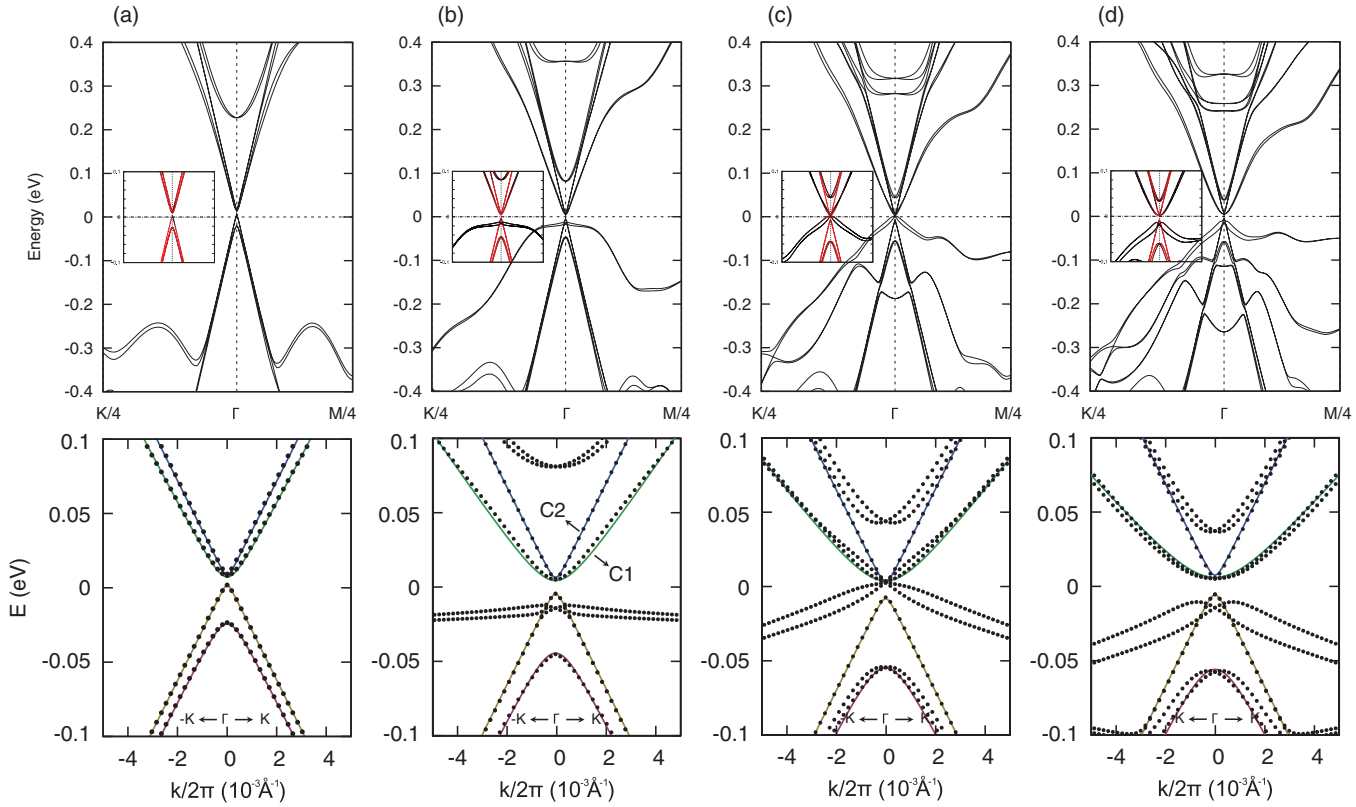

FIG. 2. (Color online) Band structures of epitaxial graphene on top of Sb_2Te_3 slab (a) 1QL, (b) 2QL, (c) 3QL, and (d) 4QL along K-Γ-M direction. The insets in the upper panels detail the electronic states from graphene (red lines) and from TI (black lines) near the Fermi level (zero energy). The lower panels show corresponding band structures along K-Γ-K direction with dots representing first-principles calculations and lines the fitting to the tight-binding Hamiltonian for graphene.

The first term is the nearest-neighbor hopping term, and the second term is the intrinsic SOC with a coupling strength $V_{\rm SO}$ with $\vec{\sigma} = (\sigma_x, \sigma_y, \sigma_z)$ being the Pauli matrices, i and j referring to next-nearest neighboring sites that have a common nearest neighbor k connected by vectors $\vec{d}_{ik}$ and $\vec{d}_{kj}$. The third and fourth terms are the Rashba SOC due to an electric field normal to the substrate and an in-plane electric field in the substrate, respectively, with i and j referring the nearest neighbors. The parameters for intrinsic spin-orbit, normal, and in-plane Rashba spin-orbit interactions are $\lambda_I = 3\sqrt{3}V_{\rm so}/2$, $\Delta_{Rz} = 3V_R/2$, and $\Delta_{Rh} = 3V_{Rh}/2$, respectively. Using this Hamiltonian, we constructed the 12×12 matrix for graphene with a $\sqrt{3} \times \sqrt{3}$ $R30^\circ$ unit cell that has six basis carbon atoms (see Appendix). The lower panels of Figs. 2 and 3 show the band structure from fist-principles calculations fitted to the tight-binding model. We identified the origin of the bands by projecting the wave functions into atomic orbitals and distinguished graphene p_z bands from TI surface states. A good agreement of DFT and TB results indicates that the spin-orbit interactions in the graphene-TI heterojunction are well represented by the tight-binding model near the Γ point. As varying the SOC strength, we can clearly see the effect of SOC. From the fitting to the TB model, the band gap opening at the Dirac point is found to originate from a change in the hopping parameters between the nearest carbon atoms. Due to the substrate, the nearest-hopping parameters now become asymmetric (t and t' in the matrix as shown in the Appendix). We note that the fitting to the TB model is done in two steps: first, fitting first-principles calculations without SOC to fix the hopping parameters, and next fitting first-principles calculations with SOC to obtain the SOC parameters of graphene. In doing so, we can distinguish the effects of the hopping parameters and the SOC in the band gap opening.

Figure 4 shows the results of intrinsic and extrinsic SOC parameters obtained from fitting first-principles calculations to the TB Hamiltonian as the number of QLs is increased. In all ranges of TI slab thickness, intrinsic SOC strength is much larger than Rashba splitting by both normal and in-plane electric fields. The three parameters (λ_I, Δ_{Rz}, and Δ_{Rh}) are increased converging to about 20, 8, and 3 meV, respectively, as Sb_2Te_3 slab thickness is increased. For other atomic configurations [P2 and P3 in Fig. 1(a)], we found similar results. The SOC strength of about ∼20 meV in our calculations is significantly larger than the value of pristine graphene of about $20 \sim 50$ μeV[6–8] by more than three orders of magnitude. This finding of enhanced SOC in graphene by proximity to TI surfaces supports that graphene can work as a probe of the topological surface states by becoming a spin-Hall system. In order to check the topological phase more explicitly, we used the tight-binding parameters obtained from fitting to the results of first-prinicples calculations and calculated the Chern number of graphene on top of Sb_2Te_3, which is given as $\frac{1}{2}[\mathrm{sgn}(\delta + \lambda_I) - \mathrm{sgn}(\delta - \lambda_I)]$.[26] By changing the spin-orbit

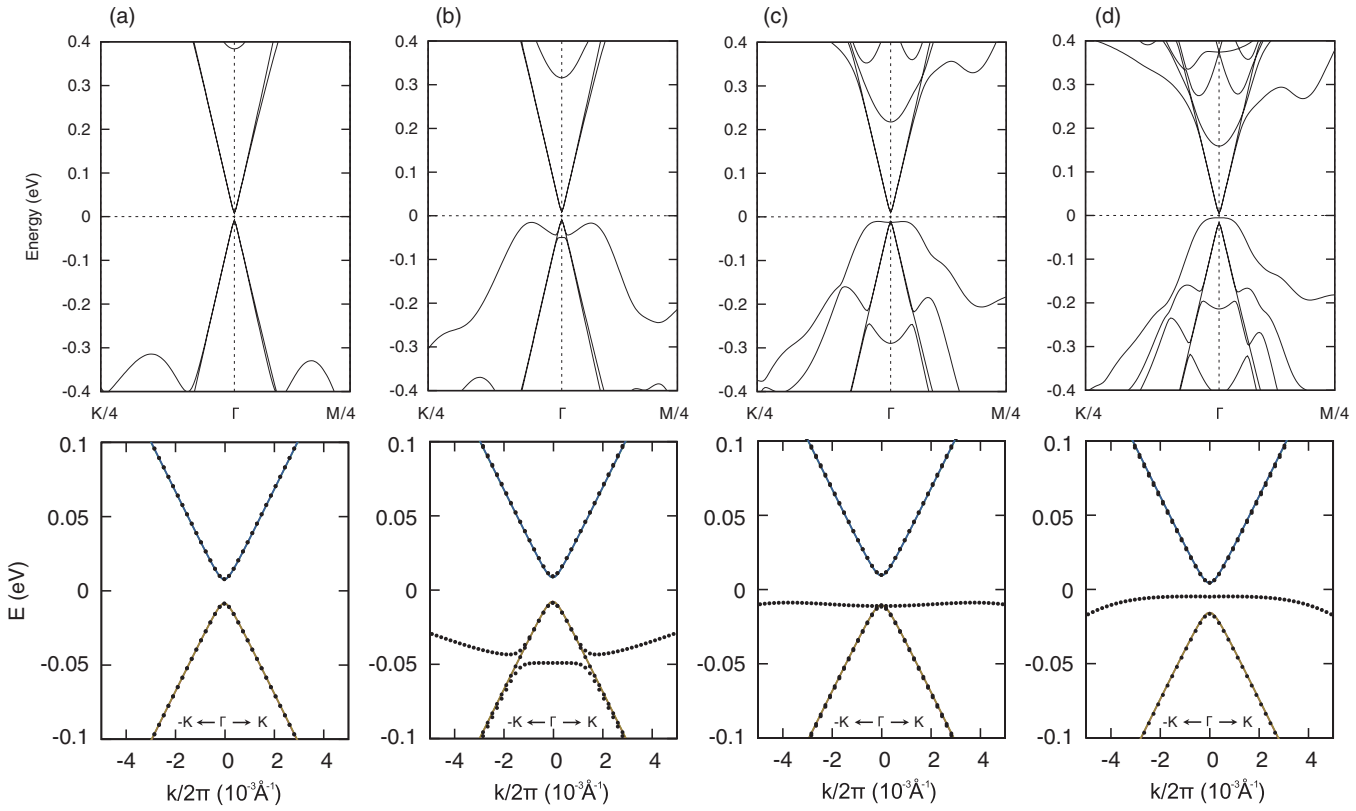

FIG. 3. (Color online) Calculated band structures without SOC of epitaxial graphene on top of Sb_2Te_3 slabs with thickness of (a) 1QL, (b) 2QL, (c) 3QL, and (d) 4QL. Lower panels are the enlargement of the electronic bands near the Γ point with the dots representing first-principles calculations and the lines the TB results.

interaction strength in our first-principles calculations, we traced the Chern number to find that graphene has a nonzero Chern number when the adjusted spin-orbit interaction is about 0.75 times the true value.

Along with the spin-orbit gap in the valence bands of about $\sim 2\lambda_I$, we observe some changes in the band dispersion of the conduction bands; the Fermi velocity is decreased to about $\leqslant 50\%$ of pristine graphene and cyclotron masses are increased as shown in Fig. 4(b). These changes will affect the electron mobility and the refraction of electron propagation. The spin helicity of the conduction bands of graphene on 5QL Sb_2Te_3 in Fig. 4(c) clearly indicates the spin-Hall phase of graphene. The density plot of a state near the Dirac point in Fig. 4(d) highlights the coupling between graphene p_z orbitals and TI surface states. The giant increase of the intrinsic spin-orbit interaction is a result of proximity of Dirac points of graphene and TI. The effective spin-orbit interaction in graphene on TI substrate can be written as[11] $\lambda_{so} = \Lambda_{so} \frac{|t_1|}{2\sqrt{3}(\varepsilon_1 - \varepsilon_\pi)^2}$, where t_1 is the hopping parameter between TI surface states, and ε_1 and ε_π are the energies of surface state and graphene p_z, orbitals, respectively (here we are mostly interested in the states near the Dirac points). When the energy levels of the Dirac point in graphene and Sb_2Te_3 are very close to each other, we expect a resonance-type enhancement in the effective spin-orbit interaction in graphene. We found that such giant enhancement does not occur when the energies of Dirac points of graphene and TI are separated greatly. Our finding of the giant spin-orbit interaction in graphene by the resonance-type proximity effect is compared to previous studies,[11] which propose orbital interactions with heavy adatoms to realize a topological phase in graphene. The adatom-induced topological phase should depend on the coverage and temperatures, but our system is free of such dependence. Also, because nondisruptive van der Waals–type interaction involves in the proximity effect, the feature of the linear dispersion of graphene will remain intact on TI substrates.

The signature of the graphene SOC enhancement can be measured by various experimental techniques. The SOC splitting will produce the Van Hove singularity in the density of states (DOS), and the spin-polarized scanning tunneling spectroscopy (STS) can probe such sharp peaks in the DOS. Figure 5(a) shows our first-principles calculations of the DOS of graphene on the 4QL Sb_2Te_3 slab with ($x = 1$) or without SOC ($x = 0$) in the Hamiltonian to resolve the features driven by the TI surface states. The van Hove singularities at about $\sim$0.05 eV below and above the Fermi level are due to the spin-orbit gap in the graphene. Grown TI substrates have a large variation in potential profile,[27] and thus graphene on TI substrates is expected to exhibit domains of the spin-Hall phase. Such puddles of the spin-Hall phase in graphene as illustrated in Fig. 5(b) can also be measured by STS. Another straightforward way to detect the helical states is to study graphene nanoribbons or edges on Sb_2Te_3. Differently from isolated graphene nanoribbons,

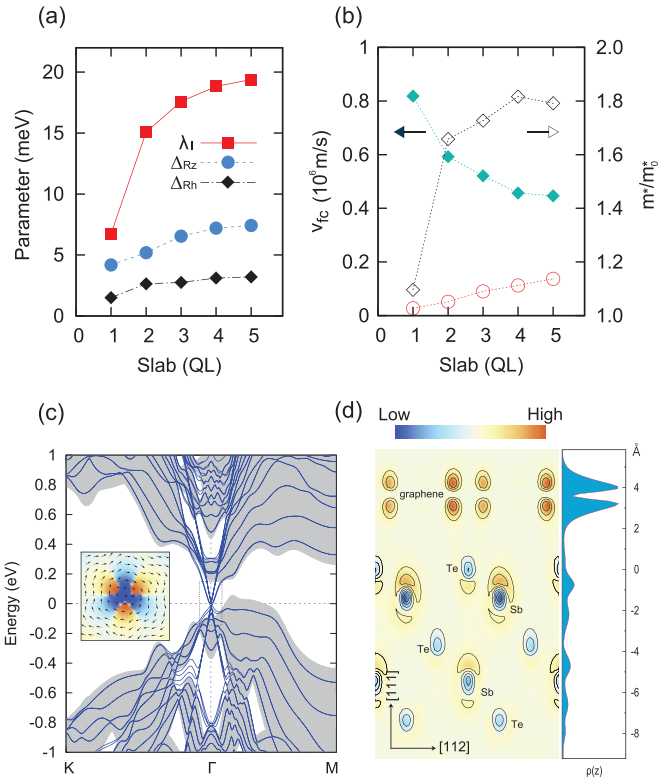

FIG. 4. (Color online) (a) Calculated results of SOC strength of graphene on top of Sb_2Te_3 slabs of 1 $\sim$ 5 QL after fitting the first-principles calculations to the tight-binding Hamiltonian. λ_I, intrinsic SOC; Δ_{Rz} and Δ_{Rh}, Rashba SOC due to normal electric field and in-plane electric field, respectively. (b) Dependence on Sb_2Te_3 substrate thickness of Fermi velocity [filled diamonds for C1 band in Fig. 2(b)] and the cyclotron mass (open diamonds and circles for the conduction bands C1 and C2, respectively, normalized to that of pristine graphene) of graphene Dirac cones. (c) Calculated band structure of epitaxial graphene on 5QL Sb_2Te_3 slab (in blue lines) superimposed with the bulk band structures projected onto the surface (shaded areas). The inset is the spin helical structure of Dirac fermions in graphene. (d) The squared wave function of a state near the Dirac point in the (112) plane and its integrated charge density $\rho(z)$ along [111] direction (right panel). The surface atomic layer of Sb_2Te_3 is at $z = 0$.

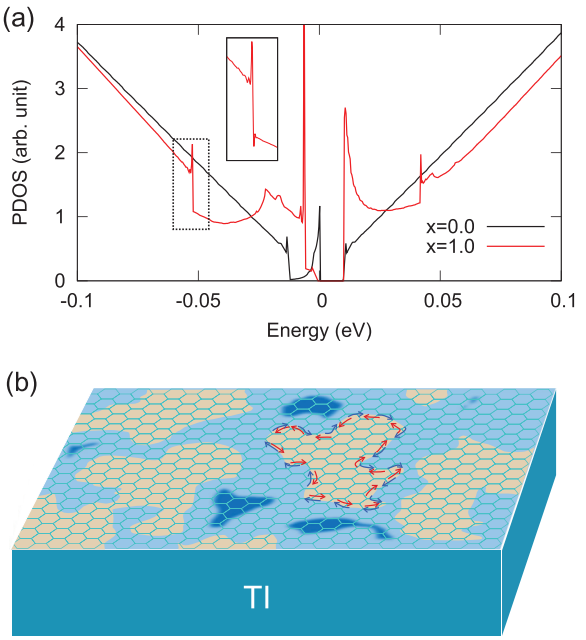

FIG. 5. (Color online) (a) First-principles calculations of density of states (DOS) of graphene on 4 QL Sb_2Te_3 with ($x = 1$) or without SOC ($x = 0$). The energy gap at the Fermi level is due to the change in the hopping parameters between the nearest carbon atoms. We observe the van Hove singularities at around $\sim$0.05 eV below and above the Fermi level, which are due to the SOC in graphene, as well as at the energy-gap edges. (b) Schematic view of the spin-polarized edge states at the phase boundary between normal and spin-Hall phases in graphene. Due to the local variation in chemical potential in Sb_2Te_3 surface, we expect the puddles of spin-Hall phase in graphene.

which have a very small spin gap for particular edge atomic structures in case of very narrow width,[28] graphene edges on top of TI will have spin-polarized conducting channels protected from atomic irregularities regardless of the width.

IV. CONCLUSION

In summary, we studied the electronic structure of epitaxial graphene on top of a Sb_2Te_3 topological insulator using first-principles calculations and tight-binding methods. We showed that a giant spin-orbit interaction of three orders of magnitude larger than the intrinsic value of graphene is induced in the epitaxial graphene so that it turns into the spin-Hall phase. This large enhancement of the spin-orbit interaction in graphene was found to be not simply because graphene is close to the surface of topological insulator but rather due to the proximity of graphene Dirac cones to that of the topological insulator. Our results demonstrate that graphene can not only be used as a probe of TI surface states but also work as fascinating spin transport structures in combination with topological insulators.

ACKNOWLEDGMENTS

We would like thank Steven G. Louie and Marvin L. Cohen for helpful discussions. This works was supported by the National Research Foundation of Korea (NRF) (Grant No. 2009-0087731, SRC Program No. 2011-0030046, and WCU Program No. R31-2008-000-10059) and by the Hydrogen Energy R&D Center, one of the 21st Century Frontier R&D Programs funded by the Ministry of Education, Science, and Technology of Korea. The authors would like to acknowledge the support from KISTI supercomputing center through the strategic support program for supercomputing application research (No. KSC-2010-C2-0008). S.H.J. also acknowledges support from National Science Foundation Grant No. DMR10-1006184 and by the Director, Office of Science, Office of Basic Energy Sciences, Materials Sciences and Engineering Division, U.S. Department of Energy, under Contract No. DE-AC02-05CH11231.

APPENDIX: 12 × 12 HAMILTONIAN MATRIX FOR A SIX-CARBON-ATOM BASIS

For the tight-binding Hamiltonian of graphene of Kane and Mele,

$$H = -t\sum_{\langle ij\rangle} c_i^\dagger c_j + \frac{iV_{SO}}{\sqrt{3}}\sum_{\langle\langle ij\rangle\rangle} c_i^\dagger \vec{\sigma}\cdot(\vec{d}_{kj}\times\vec{d}_{ik})c_j + iV_R\sum_{\langle ij\rangle} c_i^\dagger \hat{e}_z\cdot(\vec{\sigma}\times\vec{d}_{ij})c_j + iV_{Rh}\sum_{\langle ij\rangle} c_i^\dagger \hat{e}_\rho\cdot(\vec{\sigma}\times\vec{d}_{ij})c_j,$$

in the commensurate $\sqrt{3}\times\sqrt{3}$ super cell, the basis vectors are chosen as $(c_{1\uparrow},c_{2\uparrow},c_{3\uparrow},c_{4\uparrow},c_{5\uparrow},c_{6\uparrow},c_{1\downarrow},c_{2\downarrow},c_{3\downarrow},c_{4\downarrow},c_{5\downarrow},c_{6\downarrow})$ with the index standing for the six basis atoms. The Hamiltonian matrix is given as

$$\begin{Bmatrix}
0 & t+\gamma & \alpha & t'q_2^* & \alpha^* & t+\gamma^* & 0 & \beta_-^* & 0 & \beta_+^* & 0 & \beta_0 \\
t+\gamma^* & 0 & t+\gamma & \alpha & t'q_0 & \alpha^* & \beta_+ & 0 & \beta_- & 0 & \beta_0^* & 0 \\
\alpha^* & t+\gamma^* & 0 & t+\gamma & \alpha & t'q_1 & 0 & \beta_+^* & 0 & \beta_0 & 0 & \beta_-^* \\
t'q_2 & \alpha^* & t+\gamma^* & 0 & t+\gamma & \alpha & \beta_- & 0 & \beta_0^* & 0 & \beta_+ & 0 \\
\alpha & t'q_0^* & \alpha^* & t+\gamma^* & 0 & t+\gamma & 0 & \beta_0 & 0 & \beta_-^* & 0 & \beta_+^* \\
t+\gamma & \alpha & t'q_1^* & \alpha^* & t+\gamma^* & 0 & \beta_0^* & 0 & \beta_+ & 0 & \beta_- & 0 \\
0 & \beta_+^* & 0 & \beta_-^* & 0 & \beta_0 & 0 & t+\gamma^* & \alpha^* & t'q_2^* & \alpha & t+\gamma \\
\beta_- & 0 & \beta_+ & 0 & \beta_0^* & 0 & t+\gamma & 0 & t+\gamma^* & \alpha^* & t'q_0 & \alpha \\
0 & \beta_-^* & 0 & \beta_0 & 0 & \beta_+^* & \alpha & t+\gamma & 0 & t+\gamma^* & \alpha^* & t'q_1 \\
\beta_+ & 0 & \beta_0^* & 0 & \beta_- & 0 & t'q_2 & \alpha & t+\gamma & 0 & t+\gamma^* & \alpha^* \\
0 & \beta_0 & 0 & \beta_+^* & 0 & \beta_-^* & \alpha^* & t'q_0^* & \alpha & t+\gamma & 0 & t+\gamma^* \\
\beta_0^* & 0 & \beta_- & 0 & \beta_+ & 0 & t+\gamma^* & \alpha^* & t'q_1^* & \alpha & t+\gamma & 0
\end{Bmatrix},$$

where $\alpha = 3iV_{so}/2$, $\beta_+ = V_R(i+\sqrt{3})/2$, $\beta_- = V_R(i-\sqrt{3})/2$, $\beta_0 = iV_R$, and $\gamma = iV_{Rh}$. We introduce t' $(= t+\delta)$ to incorporate the change in the nearest hopping parameter due to the substrate effect.

[1] H. B. Heersche, P. Jarillo-Herrero, J. B. Oostinga, L. M. K. Vandersypen, and A. F. Morpurgo, Nature (London) **446**, 56 (2007).
[2] F. Miao, S. Wijeratne, Y. Zhang, U. C. Coskun, W. Bao, and C. N. Lau, Science **317**, 1530 (2007).
[3] X.-L. Qi, R. Li, J. Zang, and S.-C. Zhang, Science **323**, 1184 (2009).
[4] L. Fu and C. L. Kane, Phys. Rev. Lett. **102**, 216403 (2009).
[5] C. L. Kane and E. J. Mele, Phys. Rev. Lett. **95**, 226801 (2005).
[6] H. Min, J. E. Hill, N. A. Sinitsyn, B. R. Sahu, L. Kleinman, and A. H. MacDonald, Phys. Rev. B **74**, 165310 (2006).
[7] Y. Yao, F. Ye, X.-L. Qi, S.-C. Zhang, and Z. Fang, Phys. Rev. B **75**, 041401 (2007).
[8] J. C. Boettger and S. B. Trickey, Phys. Rev. B **75**, 121402 (2007).
[9] M. Gmitra, S. Konschuh, C. Ertler, C. Ambrosch-Draxl, and J. Fabian, Phys. Rev. B **80**, 235431 (2009).
[10] A. H. Castro Neto and F. Guinea, Phys. Rev. Lett. **103**, 026804 (2009).
[11] C. Weeks, J. Hu, J. Alicea, M. Franz, and R. Wu, Phys. Rev. X **1**, 021001 (2011).
[12] J. G. Checkelsky, Y. S. Hor, M. H. Liu, D. X. Qu, R. J. Cava, and N. P. Ong, Phys. Rev. Lett. **103**, 246601 (2009).
[13] Y. Xia, D. Qian, D. Hsieh, L. Wray, A. Pal, H. Lin, A. Bansil, D. Grauer, Y. S. Hor, R. J. Cava, and M. Z. Hasan, Nat. Phys. **5**, 398 (2009).
[14] D. Hsieh, Y. Xia, D. Qian, L. Wray, J. H. Dil, F. Meier, J. Osterwalder, L. Patthey, J. G. Checkelsky, N. P. Ong, A. V. Fedorov, H. Lin, A. Bansil, D. Grauer, Y. S. Hor, R. J. Cava, and M. Z. Hasan, Nature (London) **460**, 1101 (2009).
[15] D. Hsieh, Y. Xia, D. Qian, L. Wray, F. Meier, J. H. Dil, J. Osterwalder, L. Patthey, A. V. Fedorov, H. Lin, A. Bansil, D. Grauer, Y. S. Hor, R. J. Cava, and M. Z. Hasan, Phys. Rev. Lett. **103**, 146401 (2009).
[16] Y. Jiang, Y. Y. Sun, M. Chen, Y. Wang, Z. Li, C. Song, K. He, L. Wang, X. Chen, Q.-K. Xue, X. Ma, and S. B. Zhang, Phys. Rev. Lett. **108**, 066809 (2012).
[17] G. Kresse and J. Furthmüller, Phys. Rev. B **54**, 11169 (1996).
[18] J. P. Perdew, K. Burke, and M. Ernzerhof, Phys. Rev. Lett. **77**, 3865 (1996).
[19] W. Zhang, R. Yu, H. J. Zhang, X. Dai, and Z. Fang, New J. Phys. **12**, 065013 (2010).
[20] S. Grimme, J. Comput. Chem. **27**, 1787 (2006).
[21] K. Park, J. J. Heremans, V. W. Scarola, and D. Minic, Phys. Rev. Lett. **105**, 186801 (2010).
[22] O. V. Yazyev, J. E. Moore, and S. G. Louie, Phys. Rev. Lett. **105**, 266806 (2010).
[23] Y. Zhang, K. He, C.-Z. Chang, C.-L. Song, L.-L. Wang, X. Chen, J.-F. Jia, Z. Fang, X. Dai, W.-Y. Shan, S.-Q. Shen, Q. Niu, X.-L. Qi, S.-C. Zhang, X.-C. Ma, and Q.-K. Xue, Nat. Phys. **6**, 584 (2010).
[24] C. L. Kane and E. J. Mele, Phys. Rev. Lett. **95**, 146802 (2005).
[25] Y. Yang, Z. Xu, L. Sheng, B. Wang, D. Y. Xing, and D. N. Sheng, Phys. Rev. Lett. **107**, 066602 (2011).
[26] D. Sticlet, F. Piéchon, J.-N. Fuchs, P. Kalugin, and P. Simon, Phys. Rev. B **85**, 165456 (2012).
[27] H. Beidenkopf, P. Roushan, J. Seo, L. Gorman, I. Drozdov, Y. S. Hor, R. J. Cava, and A. Yazdani, Nat. Phys. **7**, 939 (2011).
[28] Y.-W. Son, M. L. Cohen, and S. G. Louie, Phys. Rev. Lett. **97**, 216803 (2006).